



# Investigation of the room-temperature photoelectron spectroscopy of type-II Weyl semimetal candidate $WTe_2$

Jian-Yang Ding<sup>1,2</sup> · Zheng-Tai Liu<sup>1,2</sup> · Zhe Huang<sup>1,3</sup> · Zhi-Cheng Jiang<sup>1</sup> · Yi-Chen Yang<sup>1</sup> · Zhong-Hao Liu<sup>1,2</sup> · Ji-Shan Liu<sup>1,2</sup> · Yan-Feng Guo<sup>3</sup> · Da-Wei Shen<sup>1,2</sup>

Received: 17 November 2022 / Revised: 1 January 2023 / Accepted: 3 January 2023 / Published online: 15 March 2023  
© The Nonferrous Metals Society of China 2023

## Abstract

Layered transition metal dichalcogenides have novel physical properties and great potential for applications. Among them,  $WTe_2$ , which has an extremely large unsaturated magnetoresistance and is theoretically predicted to be a type-II Weyl semimetal, has been extensively studied. Here, we systematically probe the electronic structure of  $WTe_2$  at room temperature using high-resolution angle-resolved photoelectron spectroscopy (ARPES). We find that temperature-driven chemical potential shift and Lifshitz transition, which is equivalent to low-energy band structures shift downward by around 50 meV, compared to the results at low temperatures. Our ARPES experimental results match well with previous theoretical calculations, implying the possible existence of type-II Weyl points near the  $\Gamma$ - $X$  axis. Also, as expected, there exists a dominantly electron-like Fermi surface instead of the one with compensated electrons and holes. Meanwhile, our ARPES results show that the flat band (FB) lying below the Fermi level ( $E_F$ ) becomes closer to the Fermi level at room temperature, which might start to dominate the transport behavior and lead to the disappearance of the unsaturated giant magnetoresistance effect. These findings not only reveal the electronic structure features of  $WTe_2$  at room temperature, but also provide new insights into the development of room-temperature topological quantum devices.

**Keywords** Weyl semimetal · Electronic structure · ARPES · Compensation effect

---

Jian-Yang Ding, Zheng-Tai Liu and Zhe Huang have equally contributed to this work.

- ✉ Zheng-Tai Liu  
ztliu@mail.sim.ac.cn
- ✉ Yan-Feng Guo  
guoyf@shanghaitech.edu.cn
- ✉ Da-Wei Shen  
dwshen@mail.sim.ac.cn

<sup>1</sup> State Key Laboratory of Functional Materials for Informatics, Shanghai Institute of Microsystem and Information Technology, Chinese Academy of Sciences, Shanghai 200050, China

<sup>2</sup> Center of Materials Science and Optoelectronics Engineering, University of Chinese Academy of Sciences, Beijing 100049, China

<sup>3</sup> School of Physical Science and Technology, ShanghaiTech University, Shanghai 201210, China

## 1 Introduction

Weyl semimetals (WSMs), possessing the critical state of ordinary insulators and topological insulators (TIs) [1, 2], carry low-energy excited Weyl fermions described by the Weyl equation. Furthermore, WSMs are classified into type-I and type-II, based on the presence or absence of Lorentz symmetry. As the first theoretically predicted type-II WSM [3, 4],  $WTe_2$  is well known to exhibit many exotic quantum phenomena, such as anisotropic chiral anomalous transport properties [5], low-temperature unsaturated giant magnetoresistance [6–8], pressurized superconductivity [9], compensation effects in three-dimensional (3D) electronic structures [10–13], topological Lifshitz phase transitions [14, 15], layer-dependent metal–insulator transition [16, 17], and monolayer quantum spin Hall effects, which have been extensively explored [18, 19].

What is clear is that the novel physical properties of  $WTe_2$  are closely related to its low-energy electronic structures. To confirm the electronic structures of type-II Weyl semimetal in  $WTe_2$ , series of angle-resolved photoelectron spectroscopy

(ARPES) studies attempted to achieve direct observation of Fermi arcs and Weyl points (WPs) [20–24]. In addition to exploring the non-trivial topological electronic structure of  $\text{WTe}_2$  materials, another brilliant ARPES experiment demonstrated that the extremely large positive unsaturated magnetoresistance in  $\text{WTe}_2$  is mostly attributed to carrier compensation which is derived from the hole and electron pockets of approximately the same size [12]. To date, although the results of transport and ARPES at low temperature confirmed that such an exotic behavior mainly stems from the perfect compensation effect of electrons and holes [11, 12] at room temperature, the detailed study of electronic structure and disappearance of unsaturated magnetoresistance remain unexplored.

In this work, we report new ARPES experimental results collected at room temperature that demonstrate a chemical potential shift and a dominantly electron-like Fermi surface instead of one with compensated electrons and holes. The photon energy-dependence spectra revealed a 3D electron pocket on the Fermi surface in  $\text{WTe}_2$ . Moreover, our results show that the flat band (FB) around  $\Gamma$  point, with a high density of states, is closer to the Fermi level ( $E_F$ ) at room temperature than at low temperature, which may contribute amounts of carriers to the transport behavior and destroy the giant unsaturated magnetoresistance effect. These findings reveal the electronic structural features of  $\text{WTe}_2$  at room temperature and provide a new experimental basis for the development and application of exotic properties in layered transition metal dichalcogenide materials.

## 2 Experimental

The high-quality single crystals of  $\text{WTe}_2$  were synthesized by the self-flux method with tellurium as the solvent as reported elsewhere [20, 25]. The room-temperature ARPES measurements were performed at the BL03U beamline of the Shanghai Synchrotron Radiation Facility (SSRF) with Scienta DA30 analyzers [26, 27]. The energy and angular resolutions were set to be better than 20 meV and  $0.02 (0.1 \text{ nm})^{-1}$ , respectively. The spot size of beamline is less than 20  $\mu\text{m}$ . The photon energies used in these measurements ranged from 20 to 50 eV. Samples were cleaved in situ along the (001) surface. During measurements, the temperature was kept at room temperature ( $T \sim 300 \text{ K}$ ), well above the Lifshitz transition point [14, 15], and the base pressure was better than  $1.33 \times 10^{-8} \text{ Pa}$ .

## 3 Results and discussion

$\text{WTe}_2$  crystallizes in the orthorhombic crystal structure with space group  $Pmn21$  and lattice parameters  $a = 0.348 \text{ nm}$ ,  $b = 0.625 \text{ nm}$ , and  $c = 1.402 \text{ nm}$ . The unit cell of  $\text{WTe}_2$  possesses two reflection symmetries: a mirror symmetry in the

$bc$  plane and a glide mirror plane formed by a reflection in the  $ac$  plane, followed by a translation by  $(0.5, 0, 0.5)$ . Figure 1a shows the side and top views of the lattice structure and a sandwich structure composed of stacked Te–W–Te along the  $c$ -axis. Due to the existence of inversion symmetry-breaking, two inequivalent Te terminal (001) surfaces (top and bottom planes in Fig. 1a) with different surface states and the same topological properties [22]. The W–W chains are connected in a zigzag pattern along the  $a$ -axis direction (Fig. 1a), and the different bond lengths of the W–Te lead to significant differences in orbital hybridization, which is accompanied by anisotropic transport behavior. Figure 1b shows the 3D-Brillouin zone (BZ) and the high-quality single crystal is shown in Fig. 1b(ii), in which a long strip extending along the W chain corresponds to the  $k_x$  direction of BZ.

The core-level spectra were acquired with  $h\nu = 100 \text{ eV}$ , and clearly show the Te-4d and W-4f peaks, as well as the Te-4d side peaks caused by the shift of chemical potential following Te termination exposure (Fig. 1c). Only two-electron pockets (Fig. 1d(ii)) were identified on the Fermi surface at room temperature (300 K), which is significantly different from that of four pairs of electron/hole pockets with same sizes at low temperatures (Fig. 1d(i)) [10, 20]. This result indicates a shift of the chemical potential to a higher energy position and is close to the previous reports, in which the measurements were carried out above the second Lifshitz transition temperature [14, 15].

Compared with ARPES measurements at low temperatures, the upward shift of the chemical potential found in the room temperature results may provide an opportunity to experimentally explore the electronic structure of  $\text{WTe}_2$  more comprehensively. Thus, we performed systematic room-temperature ARPES measurements and presented the detailed band dispersion information. As shown in Fig. 2a, b, previous theoretical results show the momentum positions of one-pair WPs ( $\text{WP}_1, \text{WP}_2$ ) with opposite chirality, which are located around 55 meV above the  $E_F$  ( $\text{WP}_1 \sim 0.052 \text{ eV}$ ,  $\text{WP}_2 \sim 0.058 \text{ eV}$ ) and close to the top of the hole bands [3]. As we all know, the Fermi arc connecting two Weyl points is an important feature of Weyl semimetallic states. Unfortunately, our results are similar to many previous measurements [22, 24]; the identification of Fermi arcs exceeds the resolution limit of our ARPES data (Fig. 1d) and cannot be confirmed by the topographic features on the Fermi surface. However, according to recent theoretical prediction results [3, 10], the momentum positions of a pair of WPs are very close to the  $\Gamma$ -X axis in the Brillouin zone ( $\text{WP}_1 \sim (0.1208 (0.1 \text{ nm})^{-1}, 0.0562 (0.1 \text{ nm})^{-1})$ ,  $\text{WP}_2 \sim (0.1226 (0.1 \text{ nm})^{-1}, 0.0238 (0.1 \text{ nm})^{-1})$ ). Next, we would like to check the band dispersion along the  $\Gamma$ -X direction in detail. In Fig. 2c, we display the corresponding ARPES intensity plot along the  $\Gamma$ -X direction, in which an electron band  $\alpha$  crosses the

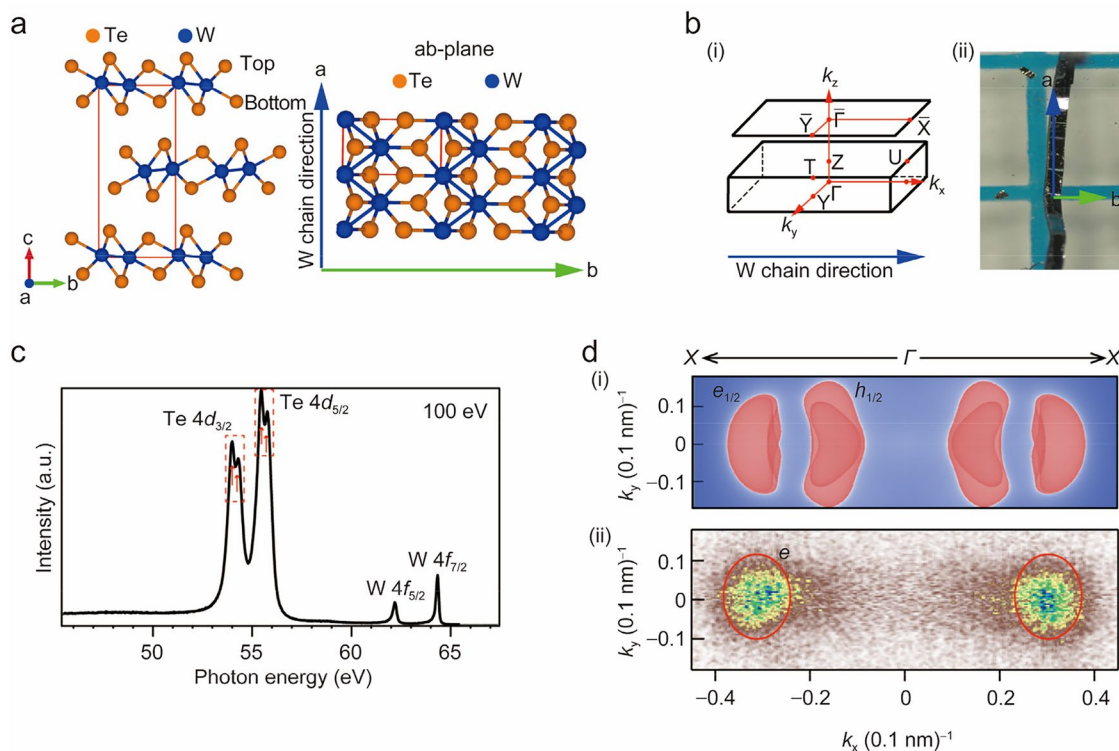


**Fig. 1** **a** The crystal structure of  $\text{WTe}_2$ . The W atoms form zigzag chains in the  $a$ -axis direction. **b** (i) Bulk and (001) surface (BZ), with high-symmetry points marked. (ii) The photograph of typical single crystal sample. **c** The core-level spectra plot taken with  $h\nu=100$  eV. **d** (i) Calculated Fermi surface in the ground state within the local

density approximation+U ( $U=2$  eV) approximation. Reproduced with the permission from Ref [10]. Copyright 2017 American Physical Society. (ii) Fermi surface of  $\text{WTe}_2$  was taken with  $h\nu=23$  eV at 300 K, and electron pockets were marked with red oval rings

Fermi level. Compared with the dispersion at low temperature, our experimental results show that  $E_F$  moves above the top of the hole band  $\beta$  at room temperature (Figs. 2c and 1d(ii)), and is shifted by about 50 meV compared to theoretical calculations (from black dotted line to green dotted line in Fig. 2b(ii)), which is not due to sample dependence and consistent with the previous ARPES results [15]. To better understand the electronic structure of  $\text{WTe}_2$ , we selected the interval along the  $\Gamma$ - $X$  axis to zoom in and appended the calculations to the intensity image. By comparing theoretical calculations with experimental measurements, it has been shown that its band structure can be perfectly captured by the calculation without any renormalization, including the electron pocket and hole pocket near  $E_F$ . However, restricted by the ARPES spectra at room temperature, the existence of the WP near the  $\Gamma$ - $X$  axis remains to be investigated.

Another interesting behavior in  $\text{WTe}_2$  is the evolution of magnetoresistance with temperature, which exhibits strong changes in different temperature ranges. The current explanation is the perfect compensation effect of the electron-hole pockets in the Fermi surface and the Lifshitz transition caused by the temperature. As shown in Figs. 3a and 1d, there are only two-electron pockets (marked by solid red

rings  $\sim e$ ) and no hole pockets (marked by pink and bright green dashed rings  $\sim h_1, h_2$ ) at room temperature, instead of one Fermi surface with compensated two-electron and four-hole pockets at low temperature (Fig. 3d), and it can be more intuitively displayed by the band dispersion along cut1 to cut3 in Fig. 3a, d. Compared to two-hole bands of  $\gamma$  and  $\beta$  across Fermi level in Fig. 3e, the guide lines for eye in Fig. 3b show two-hole bands ( $\beta$  and  $\gamma$ ) along cut1 ( $k_x=0.2$  ( $0.1 \text{ nm}^{-1}$ )) and an electron band ( $\alpha$ ) along cut2 ( $k_x=0.3$  ( $0.1 \text{ nm}^{-1}$ )). The top of the hole band  $\beta$  is located at a few meV below  $E_F$ ; by contrast, the bottom of the conduction band  $\alpha$  crosses  $E_F$  and extends nearly 0.15 eV below  $E_F$ .

In addition, for the sake of accurately distinguishing the dispersion above and below  $E_F$ , the photoemission intensity of band dispersion image is divided by the Fermi function to eliminate the temperature-broadening effect near the  $E_F$  along  $\Gamma$ - $X$ , as shown in Fig. 3c(i). The intensity image in Fig. 3c(ii) is the corresponding second-derivative plot, where one electron band and three-hole bands, named  $\alpha$ ,  $\beta$ ,  $\gamma$  and  $\delta$  near  $E_F$ , are distinguished. All of these bands can be well reproduced by the calculation and our low-temperature results (Fig. 3f), implying that the evolution of electronic structure with temperature is mainly attributed to the change



**Fig. 2** **a** Fermi surface and one Fermi arc connecting the electron and hole pockets given by first-principles calculations. Green crosses mark the position of WPs. Reproduced with the permission from Ref [3]. Copyright 2015 Nature Publishing Group. **b** (i) One-pair WPs is shown along the  $K$  (0.1208, 0.0562, 0)– $K'$  (0.1226, 0.0238, 0) direction. (ii) Band structures of  $\text{WTe}_2$  with SOC, the  $\Gamma$ – $\Sigma$  is a fraction of the  $\Gamma$ – $X$  segment from Ref. [3]. Copyright 2015 Nature Publishing Group. The bands of  $\alpha$ ,  $\beta$ , and Fermi level ( $E_F$ ) are marked. **c** The second-derivative plots of  $\Gamma$ – $X$  direction at 300 K corresponding to photoelectron intensity image. The dashed curves are the guides to the eyes for the band dispersion near  $E_F$ . **d** Band dispersion along  $\Gamma$ – $X$  and its second-derivative plot, with the calculated bands appended

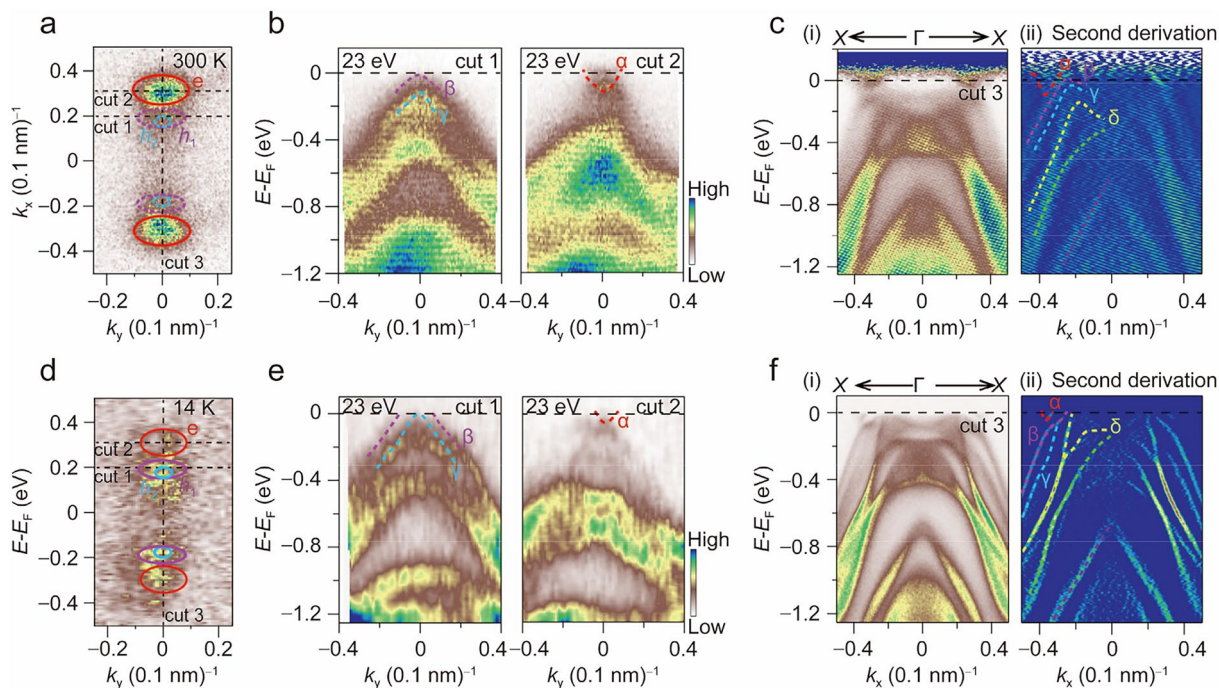
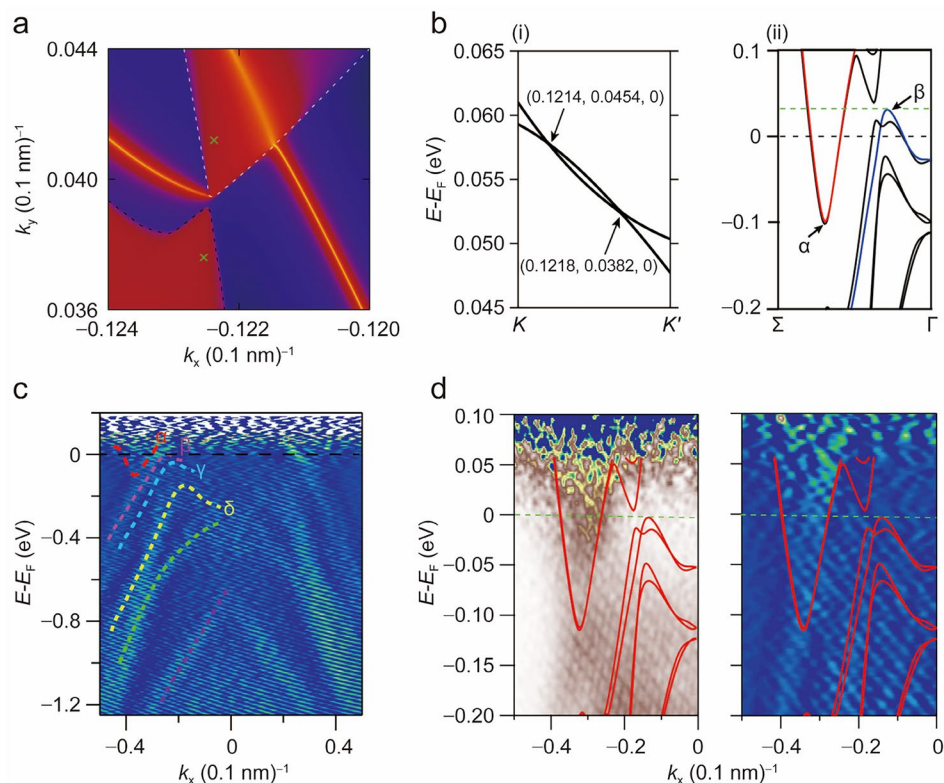


**Fig. 3** **a** Fermi surface is the same as in Fig. 1d, four-hole pockets at 0.1 eV below  $E_F$  are marked with the pink and bright green dashed rings. **b** Band dispersion along the cut1 ( $k_x=0.2$  (0.1 nm) $^{-1}$ ) and cut2 ( $k_x=0.3$  (0.1 nm) $^{-1}$ ) in Fig. 3a with  $h\nu=23$  eV. The hole and electron bands corresponding to the pockets in Fig. 3a are marked with dashed lines. **c** (i) Band structures along the  $\Gamma$ – $X$  ( $k_x$ ) direction (cut3

in Fig. 3a). (ii) The corresponding second-derivative plots. Dashed curves have been drawn on plot as a guide for band dispersion. **d** Fermi surface at 14 K, two-electron and four-hole pockets at Fermi level are marked with solid rings. **e–f** are the same as Fig. 3b,c, but at 14 K

of chemical potential. By combining photoemission spectroscopy measurements and calculation, our experimental results at room temperature confirm that the electron and hole pockets are identical in size at 50 meV below the Fermi level, which ensures a perfect electron–hole compensation at low temperature resulting in the unsaturated giant magnetoresistance effect in the ground state (Fig. 3d–f) and is consistent with the previous ARPES results at low temperatures [12]. In fact, due to the chemical potential shift upward driven by temperature, our room-temperature ARPES results along different high-symmetry directions all confirm a dominantly electron-like Fermi surface instead of the one with compensated electrons and holes.

To gain a more comprehensive understanding of the electronic structure of  $\text{WTe}_2$  at room temperature, we performed photon energy dependent ARPES measurements. Figure 4a shows the ARPES spectral intensity maps taken in the 20–50 eV range of excitation energies. Our measurements reveal periodic  $k_z$  dispersion of electronic states at the Fermi level (the  $\alpha$  dispersion in Fig. 4a), indicating that  $\text{WTe}_2$  has a 3D electronic structure. The value of the inner potential we used is  $V_0 = 9$  eV, and the corresponding photon energy for the plane of  $k_z = 0$  is 23 eV. The 3D electronic structures of  $\text{WTe}_2$  may provide channels for the interlayer coherent traveling of electron, which is also likely be related to the carrier compensation effect. Of course, it is still an open question.

Finally, we would like to examine and discuss the FB at the center of the BZ near the Fermi level. As shown in Fig. 4, we found the FB with a high density of states appears around 55 meV below  $E_F$ , which could be more clearly identified in the symmetrical momentum integrated energy distribution curves (EDCs) binned within  $\pm 0.1$   $(0.1 \text{ nm})^{-1}$  around the center point. Photon energy-dependent ARPES measurements show that this FB is barely modulated by  $k_z$  and its binding energy position is approximately fixed with different photon energies. Compared with previous results collected at 20 K, where the FB is located at 65 meV below  $E_F$  [12], our results demonstrate that this FB lies closer to the  $E_F$ . According to the Fermi–Dirac statistics mechanics, ~

$$\frac{1}{\exp\left(\frac{E-E_F}{k_B T}\right) + 1} \quad (1)$$

( $E$  is the energy of electrons,  $E_F$  the Fermi level,  $k_B$  the Boltzmann constant,  $T$  the absolute temperature), at higher temperatures, a considerable proportion of electrons in the FB near the Fermi level would be thermally excited to participate in the transport and possibly drive the turn-on behavior of the giant magnetoresistance effect, which may be the key factor for the disappearance of the unsaturated giant magnetoresistance due to low carrier density of semimetals.

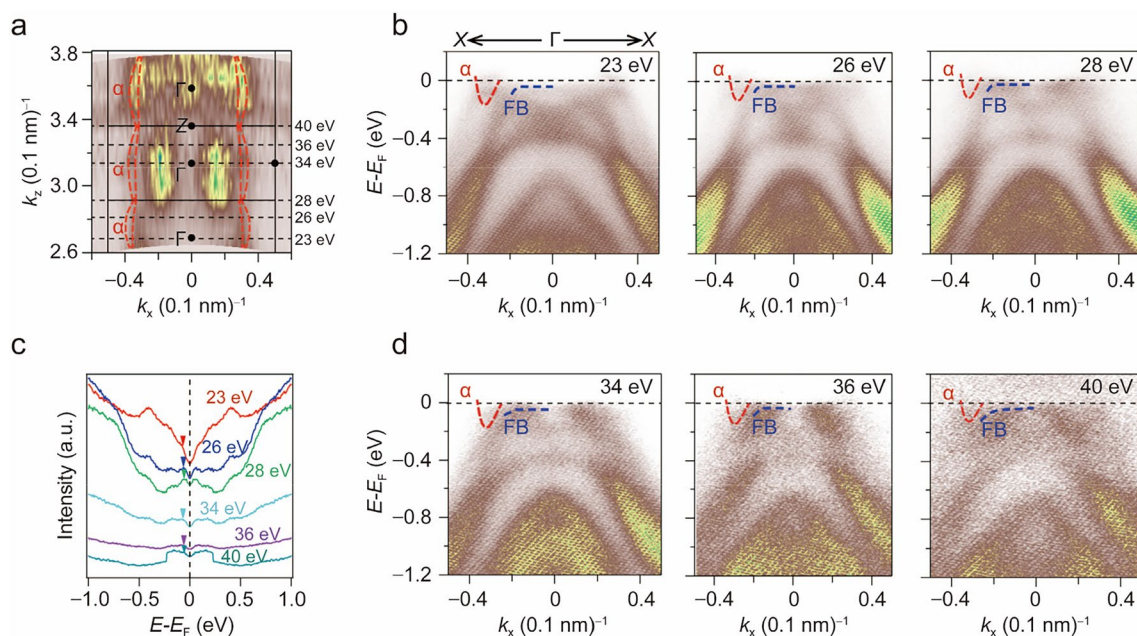


**Fig. 4** **a**  $k_x$ – $k_z$  Fermi surface taken in the 20–50 eV range of excitation energies within an energy window of  $\pm 10$  meV, and the period of  $k_z$  dispersion is assumed here to be  $2\pi/c \sim 0.45(0.1 \text{ nm})^{-1}$ . The  $k_z$  dispersion of the  $\alpha$ -electron band is marked with red dashed lines. **b**, **d** Dispersion along the  $k_x$  direction at different photon energies. The

FB and  $\alpha$  electron bands are marked by dashed lines, respectively. **c** Symmetrical EDCs integrated over the momentum range  $k_x = \pm 0.1$   $(0.1 \text{ nm})^{-1}$  at different photon energies, and binding energy positions of flat bands around the  $\Gamma$  points are marked

## 4 Conclusion

In summary, we performed detailed electronic structure measurements of  $\text{WTe}_2$  at room temperature. On the one hand, the energy band dispersion along the high-symmetry axis is in good agreement with the calculation, which provides an indirect signal for the existence of Weyl points. On the other hand, our experimental results demonstrate that the Fermi surface is fully occupied by two-electron pockets due to temperature-driven changes in chemical potential, and the electron pockets show moderate  $k_z$  dispersion. In addition, compared with the low-temperature experimental results, the FB closer to the Fermi level may contribute more to the transport and lead to the disappearance of the unsaturated giant magnetoresistance effect. Our findings not only make up for the lack of information on electronic structure in  $\text{WTe}_2$  at room temperature, but also provide experimental support for the application of novel properties in layered transition metal dichalcogenides.

**Acknowledgements** This research used resources of angle-resolved photoemission spectroscopy beamlines: BL03U beamline of the Shanghai Synchrotron Radiation Facility. This work was supported by the National Natural Science Foundation of China (NSFC, Grants No. U2032208, 12222413, 12004405), the Shanghai Science and Technology Innovation Action Plan (Grant No. 21JC1402000), the Natural Science Foundation of Shanghai (Grant No. 22ZR1473300). J. S. L. thanks the fund of Science and Technology on Surface Physics and Chemistry Laboratory (Grant No. 6142A02200102). Part of this research used Beamline 03U of the Shanghai Synchrotron Radiation Facility, which is supported by  $\text{ME}^2$  project under Contract No. 11227902 from NSFC.

**Data availability** The authors declare that the main data supporting the findings of this study are available within the paper. Extra data are available from the corresponding authors upon request.

## Declarations

**Conflict of interest** The authors declare no conflict of interest.

## References

1. Yan B, Felser C. Topological materials: Weyl semimetals. *Annu Rev Condens Matter Phys.* 2017;8(1):337.
2. Armitage NP, Mele EJ, Vishwanath A. Weyl and Dirac semimetals in three-dimensional solids. *Rev Mod Phys.* 2018;90(1):015001.
3. Soluyanov AA, Gresch D, Wang Z, Wang Z, Wu Q, Troyer M, Dai X, Bernevig AB. Type-II Weyl semimetals. *Nature.* 2015;527(7579):495.
4. Gao H, Venderbos JWF, Kim Y, Rappe AM. Topological semimetals from first principles. *Annu Rev Mater Res.* 2019;49(1):153.
5. Wang Y, Liu E, Liu H, Pan Y, Zhang L, Zeng J, Fu Y, Wang M, Xu K, Huang Z, Wang Z, Lu H, Xing D, Wang B, Wan X, Miao F. Gate-tunable negative longitudinal magnetoresistance in the predicted type-II Weyl semimetal  $\text{WTe}_2$ . *Nat Commun.* 2016;7(1):13142.
6. Ali MN, Xiong J, Flynn S, Tao J, Gibson QD, Schoop LM, Liang T, Haldolaarachchige N, Hirschberger M, Ong NP, Cava RJ. Large, non-saturating magnetoresistance in  $\text{WTe}_2$ . *Nature.* 2014;514(7521):205.
7. Zhao Y, Liu H, Yan J, An W, Liu J, Zhang X, Wang H, Liu Y, Jiang H, Li Q, Wang Y, Li XZ, Mandrus D, Xie XC, Pan M, Wang J. Anisotropic magnetotransport and exotic longitudinal linear magnetoresistance in  $\text{WTe}_2$  crystals. *Phys Rev B.* 2015;92(4):041104.
8. Cai PL, Hu J, He LP, Pan J, Hong XC, Zhang Z, Zhang J, Wei J, Mao ZQ, Li SY. Drastic pressure effect on the extremely large magnetoresistance in  $\text{WTe}_2$ : quantum oscillation study. *Phys Rev Lett.* 2015;115(5):057202.
9. Pan XC, Chen X, Liu H, Feng Y, Wei Z, Zhou Y, Chi Z, Pi L, Yen F, Song F, Wan X, Yang Z, Wang B, Wang G, Zhang Y. Pressure-driven dome-shaped superconductivity and electronic structural evolution in tungsten ditelluride. *Nat Commun.* 2015;6(1):7805.
10. Di Sante D, Das PK, Bigi C, Ergöncü Z, Gürtler N, Krieger JA, Schmitt T, Ali MN, Rossi G, Thomale R, Franchini C, Picozzi S, Fujii J, Strocov VN, Sangiovanni G, Vobornik I, Cava RJ, Panaccione G. Three-dimensional electronic structure of the type-II Weyl semimetal  $\text{WTe}_2$ . *Phys Rev Lett.* 2017;119(2):026403.
11. Caputo M, Khalil L, Papalazarou E, Nilforoushan N, Perfetti L, Ibrahim AT, Gibson QD, Cava RJ, Marsi M. Dynamics of out-of-equilibrium electron and hole pockets in the type-II Weyl semimetal candidate  $\text{WTe}_2$ . *Phys Rev B.* 2018;97(11):115115.
12. Pletikosić I, Ali MN, Fedorov AV, Cava RJ, Valla T. Electronic structure basis for the extraordinary magnetoresistance in  $\text{WTe}_2$ . *Phys Rev Lett.* 2014;113(21):216601.
13. Das PK, Di Sante D, Vobornik I, Fujii J, Okuda T, Bruyer E, Gyenis A, Feldman BE, Tao J, Ciancio R, Rossi G, Ali MN, Picozzi S, Yazdani A, Panaccione G, Cava RJ. Layer-dependent quantum cooperation of electron and hole states in the anomalous semimetal  $\text{WTe}_2$ . *Nat Commun.* 2016;7(1):10847.
14. Zhang Q, Liu Z, Sun Y, Yang H, Jiang J, Mo SK, Hussain Z, Qian X, Fu L, Yao S, Lu M, Felser C, Yan B, Chen Y, Yang L. Lifshitz transitions induced by temperature and surface doping in type-II Weyl semimetal candidate  $\text{Td-WTe}_2$ . *Physica Status Solidi (RRL). Rapid Res Lett.* 2017;11(12):1700209.
15. Wu Y, Jo NH, Ochi M, Huang L, Mou D, Bud'ko SL, Canfield PC, Trivedi N, Arita R, Kaminski A. Temperature-induced Lifshitz transition in  $\text{WTe}_2$ . *Phys Rev Lett.* 2015;115(16):166602.
16. Sakano M, Tanaka Y, Masubuchi S, Okazaki S, Nomoto T, Oshima A, Watanabe K, Taniguchi T, Arita R, Sasagawa T, Machida T, Ishizaka K. Direct observation of the layer-number dependent electronic structure in few-layer  $\text{WTe}_2$ . *arXiv preprint arXiv 2021;2103:11885.*
17. Cucchi I, Gutiérrez-Lezama I, Cappelli E, Walker SM, Bruno FY, Tenasini G, Wang L, Ubrig N, Barreateau C, Giannini E, Gibertini M, Tamai A, Morpurgo AF, Baumberger F. Microfocus laser-angle-resolved photoemission on encapsulated mono-, bi-, and few-layer  $1\text{T}'\text{-WTe}_2$ . *Nano Lett.* 2018;19(1):554.
18. Tang S, Zhang C, Wong D, Pedramrazi Z, Tsai HZ, Jia C, Moritz B, Claassen M, Ryu H, Kahn S, Jiang J, Yan H, Hashimoto M, Lu D, Moore RG, Hwang CC, Hwang C, Hussain Z, Chen Y, Ugeda MM, Liu Z, Xie X, Devereaux TP, Crommie MF, Mo SK, Shen ZX. Quantum spin Hall state in monolayer  $1\text{T}'\text{-WTe}_2$ . *Nat Phys.* 2017;13(7):683.
19. Peng L, Yuan Y, Li G, Yang X, Xian JJ, Yi CJ, Shi YG, Fu YS. Observation of topological states residing at step edges of  $\text{WTe}_2$ . *Nat Commun.* 2017;8(1):659.
20. Wang C, Zhang Y, Huang J, Nie S, Liu G, Liang A, Zhang Y, Shen B, Liu J, Hu C, Ding Y, Liu D, Hu Y, He S, Zhao L, Yu L, Hu J, Wei J, Mao Z, Shi Y, Jia X, Zhang F, Zhang S, Yang F, Wang Z, Peng Q, Weng H, Dai X, Fang Z, Xu Z, Chen C, Zhou XJ. Observation of Fermi arc and its connection with bulk

- states in the candidate type-II Weyl semimetal  $WTe_2$ . *Phys Rev B*. 2016;94(24): 241119.
21. Wu Y, Mou D, Jo NH, Sun K, Huang L, Bud'ko SL, Canfield PC, Kaminski A. Observation of Fermi arcs in the type-II Weyl semimetal candidate  $WTe_2$ . *Phys Rev B*. 2016;94(12): 121113.
  22. Bruno FY, Tamai A, Wu QS, Cucchi I, Barreateau C, Torre A, Walker SM, Riccò S, Wang Z, Kim TK, Hoesch M, Shi M, Plumb NC, Giannini E, Soluyanov AA, Baumberger F. Observation of large topologically trivial Fermi arcs in the candidate type-II Weyl semimetal  $WTe_2$ . *Phys Rev B*. 2016;94(12): 121112.
  23. Wan Y, Wang L, Kuroda K, Zhang P, Koshiishi K, Suzuki M, Kim J, Noguchi R, Bareille C, Yaji K, Harasawa A, Shin S, Cheong SW, Fujimori A, Kondo T. Selective observation of surface and bulk bands in polar  $WTe_2$  by laser-based spin-and angle-resolved photoemission spectroscopy. *Phys Rev B*. 2022;105(8): 085421.
  24. Sánchez-Barriga J, Vergniory MG, Evtushinsky D, Aguilera I, Varykhalov A, Blügel S, Rader O. Surface fermi arc connectivity in the type-II Weyl semimetal candidate  $WTe_2$ . *Phys Rev B*. 2016;94(16): 161401.
  25. Tsumura K, Yano R, Kashiwaya H, Koyanagi M, Masubuchi S, Machida T, Namiki H, Sasagawa T, Kashiwaya S. Extremely large magnetoresistance in a high-quality  $WTe_2$  grown by flux method. *J Phys Conf Series*. 2018;969(1):012134 (**IOP Publishing**).
  26. Yang YC, Liu ZT, Liu JS, Liu ZH, Liu WL, Lu XL, Mei HP, Li A, Ye M, Qiao S, Shen DW. High-resolution ARPES endstation for in situ electronic structure investigations at SSRF. *Nucl Sci Tech*. 2021;32(3):31.
  27. Sun ZP, Liu ZH, Liu ZT, Liu WL, Zhang FY, Shen DW, Ye M, Qiao S. Performance of the BL03U beamline at SSRF. *J Synchrotron Radiat*. 2020;27(5):1388.

**Publisher's Note** Springer Nature remains neutral with regard to jurisdictional claims in published maps and institutional affiliations.

Springer Nature or its licensor (e.g. a society or other partner) holds exclusive rights to this article under a publishing agreement with the author(s) or other rightsholder(s); author self-archiving of the accepted manuscript version of this article is solely governed by the terms of such publishing agreement and applicable law.